Nonlinear Model Predictive Control of Ultra-High-Purity Air Separation Units using Transient Wave Propagation Model

Jan C. Schulze[a], Adrian Caspari[a], Christoph Offermanns[a], Adel Mhamdi[a], Alexander Mitsos[b,a,c*]

[a] *Process Systems Engineering (AVT.SVT), RWTH Aachen University, 52074 Aachen, Germany.*
[b] *JARA-ENERGY, 52056 Aachen, Germany.*
[c] *Energy Systems Engineering (IEK-10), Forschungszentrum Jülich, 52425 Jülich, Germany.*

Abstract: Model reduction techniques can be used to reduce the computational burden associated with nonlinear model predictive control (NMPC). In our recent work, we introduced the transient nonlinear wave propagation model (TWPM) for reduced dynamic modeling of multi-component distillation columns with variable holdup, and demonstrated its suitability for optimization and control of single-section distillation columns and simple air separation units [Caspari et al., J. Process Contr., 2020]. We show here that the TWPM is well-suited for reduced modeling of multi-sectional ultra-high-purity distillation columns and enables real-time capable NMPC of complex process flowsheets with tight operational constraints. To demonstrate its performance and accuracy, we apply the TWPM for NMPC of an ultra-high-purity nitrogen air separation unit. We perform an in-silico closed-loop case study comprising a series of load changes. Our approach reduces CPU time by 84 %, enabling NMPC in real time.

We dedicate this article to Prof. Sebastian Engell. As he has made numerous contributions to model predictive control and its extensions, we hope that he will enjoy this article.

Keywords: Model reduction, nonlinear model predictive control, nonlinear wave propagation, cryogenic air separation, multi-section distillation column, ultra-high-purity nitrogen.

This is the authors' accepted manuscript of the following article: J.C. Schulze, A. Caspari, C. Offermanns, A. Mhamdi, A. Mitsos. Nonlinear model predictive control of ultra-high-purity air separation units using transient wave propagation model. *Computers & Chemical Engineering* 145 (2021), 107163, which was published in its final form at: DOI:10.1016/j.compchemeng.2020.107163

1 Introduction

The computational cost of dynamic optimization strongly depends on the complexity of the embedded mathematical model. It is of particular relevance in online applications such as nonlinear model predictive control (NMPC) [1]. Model reduction strategies aim at lowering this computational burden while retaining high model accuracy [1]. Distillation columns are one of the key unit operations in chemical processes. In general, mechanistic stage-by-stage modeling of these units leads to high-dimensional nonlinear systems of equations that are computationally demanding to solve [2]. Therefore, reduced models are interesting for NMPC of flowsheets including distillation columns with many stages, cf. [3]. While linear MPC is the more established control method for operating chemical processes, such as air separation units (ASUs), NMPC facilitates process operation on a wider range of production rates [4]. Capturing the nonlinear plant behavior is of particular importance when considering economic flexible operation of the plant with significant load changes as, e.g., required for demand-side management [5, 6]. Hence, we aim at deriving a real-time capable NMPC using a nonlinear reduced dynamic controller model.

Among the model reduction techniques for distillation columns, collocation methods [7, 8], compartment modeling [9, 10] and nonlinear wave propagation models (WPM) [11–13] are the most prevalent strategies

*Corresponding author: amitsos@alum.mit.edu

adopted in the literature. WPMs have several strengths over the other reduction approaches. First, the number of differential and algebraic variables is small and independent of the number of column stages, making WPM particularly suited for large distillation columns. Second, as opposed to collocation and compartment methods, the number of model parameters is small and all parameter values can be determined from steady-state data only. In addition, modeling decisions such as the selection of suitable collocation points are not present, leading to comparably small modeling effort. However, due to strong assumptions under which the partial-differential component balances can be solved analytically, WPMs show good predictions only for near-ideal mixtures and columns. Another limitation of classic WPMs is their restriction to constant holdups. To overcome the latter limitation, we recently extended the multi-component WPM of Kienle [14] by adding a global hydraulic correlation [15]. This idea can be regarded as a combination of nonlinear wave theory and compartment modeling and enables the use of the WPM in transient process operation. Thus, we term our approach transient wave propagation model (TWPM).

The mentioned reduction techniques have been applied to a number of works on dynamic optimization and control of high-purity distillation columns. Most studies investigated the WPM for control of single columns with binary or pseudo-binary systems [3, 16–24]. In addition, reduced dynamic modeling of multi-component distillation columns or distillation columns with multiple sections has been the subject of a number of contributions. Han et al. [25] used the WPM to implement a controller for the semi-continuous transition phase of a start-up procedure for a multi-sectional two-column configuration and a pseudo-binary mixture. Cao et al. [26] employed the collocation method for reduced modeling and offline economic dynamic optimization of the multi-sectional distillation columns in an ASU. Bian et al. [2] developed a compartment model for the multi-section column of an ASU. The model was later combined with DAE structure exploitation strategies in an NMPC case study by Chen et al. [4]. Kumar and Daoutidis [27] performed singular perturbation analysis to derive a low-order nonlinear model for a ternary distillation column with two sections and large internal flows. Grüner et al. [28] and Schwarzkopf [29] employed the multi-component WPM of Kienle [14] for wave position control in a ternary multi-section distillation column by means of NMPC. By contrast, few works have considered the control of entire process flowsheets using reduced distillation column models. In our previous works, we used a hybrid mechanistic data-driven compartment model and the TWPM for NMPC of complete ASU processes including a single-section distillation column [15, 30].

While reduced dynamic modeling and control of multi-section distillation columns and the application to simple flowsheet topologies have been presented in the literature, the combination of both tasks, i.e., reduction-based NMPC of complex processes featuring multi-sectional distillation columns, is missing. However, process control of complex flowsheets is important for industrial applicability of the model reduction approaches. In this work, we investigate the application of the TWPM for NMPC of an ultra-high-purity cryogenic ASU comprising a bi-sectional ternary column with side streams and multiple heat exchangers. We select this process to demonstrate the suitability of the TWPM for reduced modeling of ultra-high-purity multi-section distillation columns. Further, we show that the TWPM enables real-time capable NMPC of an entire complex process flowsheet with tight operational constraints. To this end, we develop a reduced ASU model and demonstrate its application in a closed-loop NMPC case study considering a series of load changes. We use an NMPC embedding a mechanistic process model as benchmark to assess the performance and computational benefit from reduced modeling.

The remainder of the article is structured as follows: Section 2 presents the ASU investigated in the case study and a mechanistic process model. In Section 3, we develop a reduced process model. Section 4 introduces the NMPC case study and presents a discussion of the results. The manuscript closes with conclusions and outlook in Section 5.

2 Ultra-high-purity Air Separation Unit

Ultra-pure nitrogen (N_2) is an industrial gas characterized by the requirement for an extremely small impurity content in the ppb (parts per billion) range [31]. In this study, we consider an energy-integrated ultra-high-purity ASU similar to the one introduced in the patent specification [32]. We discuss the key features of the process below. Further, we present a corresponding mechanistic dynamic process model.

2.1 Process Description

The topology of the cryogenic ASU investigated is illustrated in Fig. 1. The process produces pressurized ultra-pure gaseous nitrogen (PGAN). Compressed and pre-purified air at 10 bar and ambient temperature enters the process (1) and is successively cooled in two consecutive heat exchangers (HX1, HX2) to superheated vapor close to the saturation point (2). The chilled air stream is fed into a bi-sectional distillation column in which the least volatile component, nitrogen, accumulates at the top. We specify process parameters and unit sizing to produce nitrogen with max. 10 ppb impurity content. The rectifying section of the distillation column has 79 stages, while the stripping section has 20 stages. Liquid reflux at the column top is provided by condensing a part of the exiting vapor stream in a heat integrated condenser (HX3). A fraction of the liquid outlet of the column feed stage is withdrawn (3), subcooled (HX4), expanded in a throttle valve to 5.1 bar, fully evaporated (HX3), boosted in a compressor (COMP), cooled (HX2) and reintroduced at the column bottom (4) to increase the nitrogen yield. The boosted stream (4) leaves heat exchanger HX2 in two-phase state containing a minor fraction of liquid. The two less volatile components argon and oxygen accumulate at the column bottom and are discharged as waste stream (9).

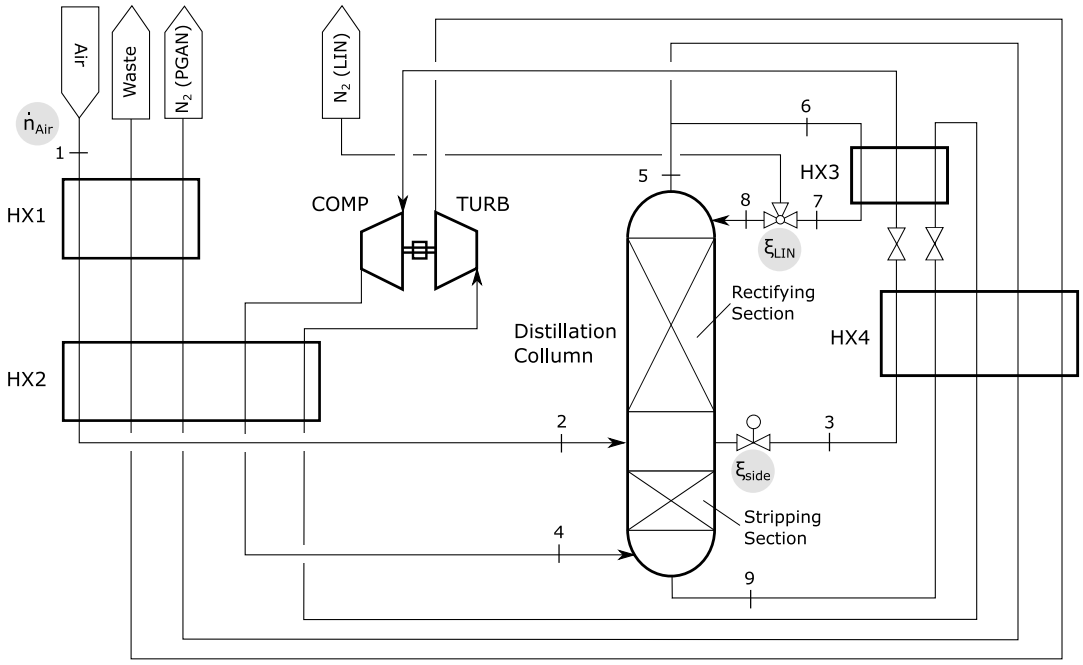

Fig. 1: Process flowsheet based on patent specification [32]. Manipulated variables highlighted by gray circles.

Both product and waste streams are used as cooling agents in the heat-integrated process. The waste stream (9) is subcooled in HX4, expanded to 4.1 bar, fully evaporated in HX3 and heat integrated in HX4, HX2 and HX1. Further, the waste stream is expanded in a turbine (TURB) to 1.2 bar in order to provide power for compression of the withdrawn stream (COMP). Turbine and compressor are mechanically coupled and excess power generated in the turbine is dissipated in an energy dissipative break. A part of the liquid reflux stream exiting the condenser (7) can be discharged as liquid nitrogen product $\dot{n}_{\mathrm{LIN}}$. Using the proposed design specifications, the nitrogen yield in nominal steady-state operation is 81.9 %. The nitrogen yield relates the amount of nitrogen in the feed air stream $\dot{n}_{\mathrm{N_2}}^{\mathrm{Air}}$ and the product stream $\dot{n}_{\mathrm{PGAN}}$. The manipulated variables (MVs) of the process are (i) the feed air stream $\dot{n}_{\mathrm{Air}}$, (ii) flow split factor of the discharged liquid nitrogen stream ξ_{LIN}, and (iii) flow split factor ξ_{side} as indicated in Fig. 1. The MV ξ_{side} specifies the fraction of liquid exiting the feed stage that is withdrawn as side stream (3).

2.2 Mechanistic Process Model

We develop a mechanistic full-order process model (FOM) as plant surrogate and use it to benchmark the computational cost and control performance of an NMPC. The FOM comprises detailed mechanistic

models of all process components that are similar to the models presented in [5]. Air is modeled as ternary mixture of the low-boiling component nitrogen (N_2), medium-boiling component argon (Ar), and high-boiling component oxygen (O_2). The cryogenic distillation column is represented through stage-by-stage mechanistic modeling, including MESH equations for each column tray. Due to the fast dynamics of compressor, turbine and total condenser (HX_3), we employ quasi-stationary models for these units. The remaining heat exchangers (HX1, HX2, HX4) are modeled by means of 1D distributed dynamic models. Details are provided in the supplementary information.

3 Model Reduction using TWPM

Based on the FOM, a reduced process model employing the TWPM is developed in this section. First, we provide a brief description of the underlying theory. A detailed presentation of the TWPM is given in our previous work [15]. We then present a reduced model for the multi-sectional distillation column. Finally, we perform parameter estimation to determine the TWPM parameter values. We use the reduced process model as controller model for NMPC in Section 4.

3.1 Transient Nonlinear Wave Propagation Model

The concentration profile x_i of a chemical species $i \in \{1, ..., N_c\}$ in the liquid phase of a distillation column is computed by means of a superposition of $N_c - 1$ concentration waves k:

$$x_i(z, s^{(1)}, ..., s^{(N_c-1)}) = x_i^{(1)} + \sum_{k=1}^{N_c-1} \frac{x_i^{(k+1)} - x_i^{(k)}}{1 + \exp(-\rho^{(k)}(z - s^{(k)}))}, \quad \forall i = 1, ..., N_c - 1, \tag{1}$$

where z is the spatial coordiante along the longitudinal axis of the distillation column, $\rho^{(k)}$ is the wave slope, and $s^{(k)}$ is the coordinate of the moving front of wave k. The variables $x_i^{(k)}$ and $x_i^{(k+1)}$ represent the asymptotic values of the wave k for $z \to -\infty$ and $z \to \infty$, respectively. The vapor composition is calculated in a similar manner:

$$y_i(z, s^{(1)}, ..., s^{(N_c-1)}) = f_i(\boldsymbol{x}^{(1)}) + \sum_{k=1}^{N_c-1} \frac{f_i(\boldsymbol{x}^{(k+1)}) - f_i(\boldsymbol{x}^{(k)})}{1 + \exp(-\rho^{(k)}(z - s^{(k)}))}, \quad \forall i = 1, ..., N_c - 1, \tag{2}$$

where the equilibrium function is defined as:

$$f_i(\boldsymbol{x}^{(k)}) = \frac{\alpha_i x_i^{(k)}}{1 + \sum_{j=1}^{N_c-1} (\alpha_j - 1) x_j^{(k)}} . \tag{3}$$

The continuous wave propagation theory is also applicable to staged columns [33]. We define $z = 0$ and $z = 1$ to represent the column bottom and top, respectively, and consider a set $\mathcal{Z}$ of discrete values of z to account for the staged realization of the column. The parameter α_i is the constant relative volatility of the component i with respect to the high-boiling component, here oxygen. The asymptotic values $x_i^{(k)}$ and $x_i^{(k+1)}$ of different waves are mathematically coupled through compatibility conditions, cf. [14]. The wave slope $\rho^{(k)}$ is calculated as:

$$\rho^{(k)} = \frac{B \sum_{j=1}^{N_c-1} (\alpha_j - 1)(x_j^{(k+1)} - x_j^{(k)})}{1 + \sum_{j=1}^{N_c-1} \frac{1}{2}(\alpha_j - 1)(x_j^{(k+1)} + x_j^{(k)})} . \tag{4}$$

Herein, the model parameter B can be interpreted as dimensionless mass transfer coefficient [14]. Note that in the model as presented above, the asymptotic values $x_i^{(k)}$ and wave slopes $\rho^{(k)}$ generally change with time as a reaction to varying amount and composition of the liquid and vapor feed streams. The mean concentration $\bar{x}_i$ of a chemical species in the column used for global mass and energy balances is obtained from integral summation:

$$\bar{x}_i = \int_0^1 x_i(z, s^{(1)}, ..., s^{(N_c-1)}) \, \mathrm{d}z . \tag{5}$$

We formulate a global linear hydraulic correlation for the entire column section to account for transient liquid holdup:

$$\dot{n}_{\mathrm{L,out}} = \bar{k}_d \cdot n_{\mathrm{total}} \ , \tag{6}$$

where $\bar{k}_d$ is the global hydraulic coefficient and n_{total} the total molar holdup of the column section. In addition to Eqs. (1) to (6), we formulate global energy and mass balances for the column section. Due to the fast temperature dynamics, the energy balance is written in quasi-stationary form. A complete presentation of the model equations can be found in [15]. The TWPM is a low-order model as it comprises N_c differential states only. These differential variables are the total molar column hold-up n_{total} as well as $N_c - 1$ molar amounts of species n_i. The latter states are directly correlated with the wave positions $s^{(k)}$ and mean concentrations $\bar{x}_i$.

3.2 Reduced Controller Model

The intermediate feed/withdrawal tray divides the distillation column into two sections. Consequently, we formulate a reduced-order model by combining two TWPMs with mechanistic models for the feed-withdrawal and bottom tray as illustrated in Fig. 2. Rigorous modeling of the feed tray and bottom tray

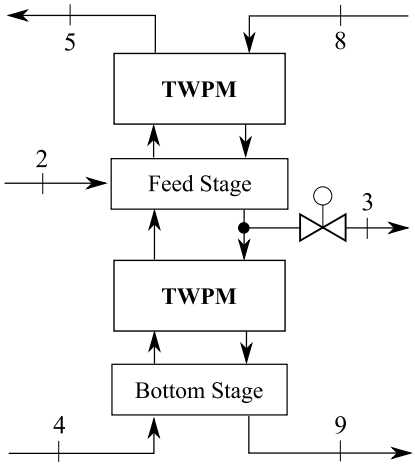

Fig. 2: Illustration of the configuration of TWPMs and mechanistic feed and bottom stage models.

provides a flash calculation for the superheated feed stream (2) and two-phase bottom feed stream (4), respectively. Hence, all streams entering the two TWPM blocks are in saturated vapor or liquid state. We do not investigate the reduction of the heat exchanger, turbine and compressor models herein.

As the equations in the TWPM are derived under the assumption of constant relative volatilities, the approach is only valid for near-ideal mixtures. From FOM simulation of the process in nominal operation, we observe relative volatilities within a narrow range, $\alpha_{\mathrm{N_2}} \in [2.69, 2.71]$ and $\alpha_{\mathrm{Ar}} \in [1.24, 1.26]$, and conclude the applicability of TWPM to both sections. This nominal operating point is defined as steady state corresponding to $\dot{n}_{\mathrm{Air}} = 800\,\mathrm{mol\,s^{-1}}$, $\xi_{\mathrm{side}} = 0.505$ and $\xi_{\mathrm{LIN}} = 0.001123$, which leads to 10 ppb impurity. The reduced process model comprises a set of 62 differential and 5 202 algebraic equations, where the three-component TWPMs and models for feed and bottom tray involve three differential equations each. The remaining 50 differential equations are due to the dynamic modeling of the heat exchangers. By contrast, the mechanistic process model has 350 differential and 14 205 algebraic equations, including 300 differential equations of the mechanistic stage-by-stage column model. This demonstrates the significant model reduction capabilities of the wave propagation approach.

3.3 Parameter Estimation

For each TWPM, the dimensionless mass transfer coefficient B, relative volatilities $\alpha_{\mathrm{N_2}}$ and α_{Ar}, and the global hydraulic coefficient $\bar{k}_d$ have to be specified. For their estimation, we use as data set the

concentration profiles and tray holdups from an FOM simulation at the nominal steady state. Even though the model parameter values are identified from data of a single steady state only, we expect the column model to be valid over a wide range of operating conditions. This is a particular strength of the TWPM as discussed in the introductory section. However, due to idealized modeling assumptions, plant-model mismatch may occur far from the nominal point. One possible strategy to tackle such a behavior is the consideration of multiple steady-states for parameter estimation. However, as we show in this work, the model identified for a single steady state is sufficient for control purposes.

The global hydraulic coefficient $\bar{k}_d$ is determined directly from the total liquid holdup $n_{\mathrm{L,total}}$ and the exiting liquid flow $\dot{n}_{\mathrm{L,out}}$ of the column section:

$$\bar{k}_d = \frac{\dot{n}_{\mathrm{L,out}}}{n_{\mathrm{L,total}}} \,. \tag{7}$$

For the identification of the remaining parameter values, we individually fit the reduced models of rectifying and stripping sections to the steady-state concentration profiles. The parameter B is determined by means of least-squares optimization. Values for the parameters $\alpha_{\mathrm{N_2}}$ and α_{Ar} may be obtained either from averaging the relative volatilities from the data set over all trays, or from a least-squares fitting procedure [15]. Here, we allow the optimizer to determine constant relative volatilities $\alpha_{\mathrm{N_2}}$ and α_{Ar} within the range of values observed in the FOM, i.e., $\alpha_{\mathrm{N_2}} \in [2.69, 2.71]$ and $\alpha_{\mathrm{Ar}} \in [1.24, 1.26]$.

While the classical least-squares method provides reasonable parametric values for the stripping section, the parameter values for the rectifying section obtained from this approach were found to be unsatisfactory. Since the concentration profiles range over several orders of magnitude, considerable deviation from the data points was found in the ultra-high purity part. To improve the model quality in this range, we scale all errors by the impurity content from the data set, cf. Eq. (8). Thereby, we obtain an improved fit over the full spectrum of concentrations. The scaled objective function of the parameter estimation problem for the rectifying section thus becomes:

$$\Phi_{\mathrm{LSQE}} = \sum_{j=1}^{N_\mathrm{t}} \left(\frac{x_{j,\mathrm{N_2}}^{\mathrm{TWPM}} - x_{j,\mathrm{N_2}}^{\mathrm{Data}}}{1 - x_{j,\mathrm{N_2}}^{\mathrm{Data}}} \right)^2 + \left(\frac{x_{j,\mathrm{Ar}}^{\mathrm{TWPM}} - x_{j,\mathrm{Ar}}^{\mathrm{Data}}}{1 - x_{j,\mathrm{N_2}}^{\mathrm{Data}}} \right)^2 \,, \tag{8}$$

where N_t is the number of stages of the column section. We further add the following constraint to the parameter estimation problem of the rectifying section:

$$x_{N_\mathrm{t},\mathrm{N_2}}^{\mathrm{TWPM}} - x_{N_\mathrm{t},\mathrm{N_2}}^{\mathrm{Data}} \leqslant 0 \,, \tag{9}$$

to prevent overestimation of product purity by the reduced column model in the nominal operating point.

3.4 Parameter Estimation Results

We formulate the steady-state parameter estimation problems as dynamic optimization problems with terminal cost and solve them offline with our open-source optimization package DyOS [34]. We specify relative integration and optimization tolerances of 10^{-8} and 10^{-6}, respectively, and a sufficiently long horizon of 1000 h to reach a steady state at the final time. The estimated parameter values are listed in Table 1. The resulting stationary concentration profiles at the nominal operating point are presented in Fig. 3.

As known from the literature, the parametric values for coefficients B are in the order of magnitude of the number of stages of the respective column section [14]. The estimated parameter values lead to accurate prediction of the nitrogen concentrations in each column section, Figs. 3a, 3c and 3e. The relative deviation of the nitrogen profiles from the data points is small with mean μ and standard deviation σ in both sections below 0.9 % and 1.6 %, respectively. However, the argon profiles in both column sections exhibit significant relative errors. Especially the argon concentration bulge in the top section is strongly overestimated by a factor of roughly 2.5, Fig. 3b. Manipulation of the relative volatilities outside the range of physical values from FOM simulation did not improve this mismatch. Investigation of the internal vapor and liquid flows reveals a variation by 14 % in the bulge region, i.e. violation of the modeling

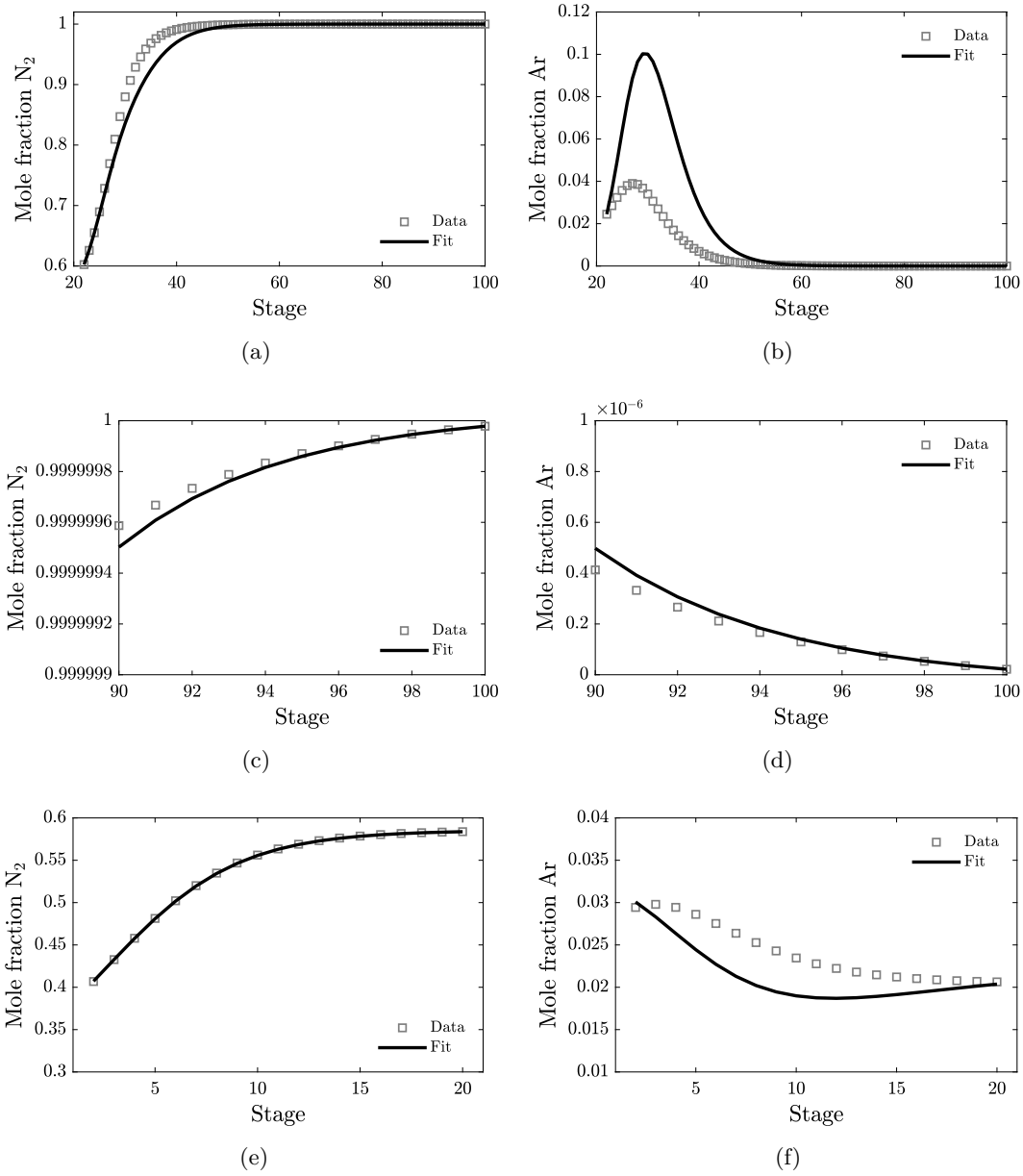

Fig. 3: Concentration prediction by the reduced models at nominal steady state. Tray numbering from bottom to top. Extrapolation indicated by dotted line. (a) + (b): Rectifying section. (c) + (d): Top ten stages of rectifying section. (e) + (f): Stripping section.

Table 1: Model parameters for rectification (I) and stripping section (II) of the distillation column. Number of stages N_t for comparison.

	N_t	B	$\alpha_{\mathrm{N_2}}$	α_{Ar}	$\bar{k}_d$
Section I	79	135.34	2.71	1.26	$0.0079\,\mathrm{s}^{-1}$
Section II	20	19.61	2.71	1.26	$0.0356\,\mathrm{s}^{-1}$

assumptions of the TWPM. We expect a reduction of the observed mismatch through rigorous stage-by-state modeling of the argon bulge region. This would, however, lead to a more complex model and thereby increase the computational cost of NMPC. Another alternative is using a more complex wave propagation approach accounting for enthalpy effects, as presented in [35]. However, the enthalpy calculation that would be required for each tray similarly results in a significant increase in model complexity.

Here, we accept the observed model inaccuracy when using a single TWPM per column section as the effect on the nitrogen profiles, i.e. the target component, appears to be small and the model to be sufficently accurate for control purposes. The imprecise reproduction of the argon data points is generally expected to affect the composition of the withdrawn side stream and bottom stream, thereby affecting the enthalpy calculations relevant for the heat exchangers. However, as our control case study in Section 4 shows, the observed model mismatch does not have a noticable effect on the control performance.

4 NMPC Case Study

The performance of NMPC embedding the reduced TWPM process model is investigated in a closed-loop control case study in-silico.

4.1 NMPC Formulation

We investigate an NMPC scenario that aims at tracking a given product demand profile. The NMPC repeatedly solves a dynamic optimization problem (DOP) on a sampling grid of interval length Δt_s and implements the first control move to the process [36]. We formulate the DOP as follows:

$$\min_{\boldsymbol{x},\boldsymbol{u}} \quad \int_{t_0}^{t_\mathrm{f}} \ell(\boldsymbol{x}(\tau),\boldsymbol{u}(\tau),\tau)\,\mathrm{d}\tau \tag{10a}$$

$$\text{s.t.} \quad \boldsymbol{M}\dot{\boldsymbol{x}}(t) = \boldsymbol{f}(\boldsymbol{x}(t),\boldsymbol{u}(t)),\ \forall t \in \mathcal{T}, \tag{10b}$$

$$\boldsymbol{x}(t_0) = \hat{\boldsymbol{x}}, \tag{10c}$$

$$\boldsymbol{x}(t) \in \mathcal{X},\ \boldsymbol{u}(t) \in \mathcal{U},\ \forall t \in \mathcal{T}, \tag{10d}$$

where $\boldsymbol{x} : \mathcal{T} \to \mathbb{R}^{n_x}$ are the state variables, $\boldsymbol{u} : \mathcal{T} \to \mathbb{R}^{n_u}$ are the manipulated variables, $\mathcal{T} = [t_0, t_\mathrm{f}]$, where t_0 and t_f are the initial and final time, respectively. Accordingly, $T_\mathrm{p} = t_\mathrm{f} - t_0$ is the prediction horizon. The objective function, Eq. (10a), is of Lagrange type with running cost function $\ell : \mathbb{R}^{n_x} \times \mathbb{R}^{n_u} \times \mathcal{T} \to \mathbb{R}$. The matrix $\boldsymbol{M} \in \mathbb{R}^{n_x \times n_x}$ is the coefficient matrix of the differential-algebraic system of equations, Eq. (10b). Condition (10c) initializes the dynamic problem with the current process state $\hat{\boldsymbol{x}}$, which is obtained from state estimation. The sets $\mathcal{X}$ and $\mathcal{U}$, Eq. (10d), specify the admissible states $\boldsymbol{x}(t)$ and controls $\boldsymbol{u}(t)$, respectively.

To implement the tracking NMPC, the running cost ℓ in the DOP (10) is specified as quadratic function penalizing the deviation from the production target:

$$\begin{aligned}\ell(\boldsymbol{x}(t),\boldsymbol{u}(t),t) := \quad & \omega_1 \cdot (\dot{n}_\mathrm{PGAN}(t) - \dot{n}_\mathrm{PGAN,sp}(t))^2 \\ & + \omega_2 \cdot (x_{\mathrm{N_2}}^{\mathrm{PGAN}}(t) - x_{\mathrm{N_2,sp}}^{\mathrm{PGAN}})^2 \\ & + \omega_3 \cdot \dot{n}_\mathrm{LIN}(t)^2\,.\end{aligned} \tag{11}$$

Herein, $\dot{n}_\mathrm{sp}^\mathrm{PGAN}$ is the product demand. Tracking the product demand profile is the primary objective of the controller. However, since over-purification in a column is commonly associated with economic

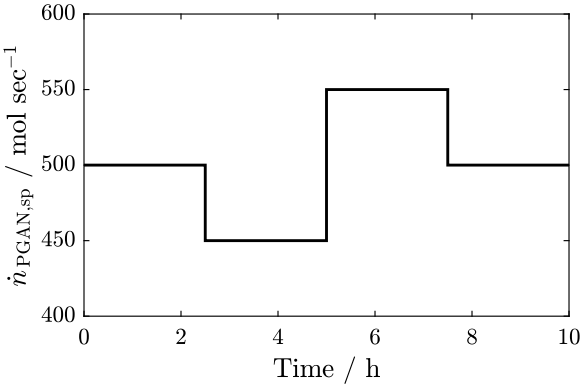

Fig. 4: Product demand profile investigated in the case study.

loss and thus undesirable [37], a second cost term is added, which penalizes the deviation of product quality from the constant setpoint $x^{\mathrm{PGAN}}_{\mathrm{N_2,sp}}$. Note that satisfaction of the requested product quality is independent of this second cost term and ensured by means of a hard quality constraint in the DOP (10). Finally, we include a cost term for the liquid nitrogen stream (LIN) to minimize over-production and extensive discharge for improved tracking. The coefficients ω_i represent tuning parameters of the controller specifying the trade-off between tracking performance and economic criteria. The tuning of the NMPC is presented in Section 4.2.

We implement a piecewise-linear continuous control parameterization with bounds on the time derivatives Δu_i of the MVs. We allow sufficiently large values of Δu_i to operate the process with smooth but fast control action, cf. Section 4. The control grid is a structured grid with interval length $\Delta t_{\mathrm{u}} = \Delta t_{\mathrm{s}}$ for $t \in [t_0, t_0 + T_{\mathrm{u}}]$, and a single control interval on the remaining prediction horizon. We apply a shift initialization strategy for the MVs. All path constraints are evaluated on the sampling grid, which is assumed to be sufficiently fine for the process investigated.

We employ an extended Kalman filter (EKF) for state estimation [38], i.e., to determine online the current holdups and concentrations of the two column sections and the feed and bottom tray of the reduced model. We assume that the flow rates and compositions of the product stream (PGAN), $\dot{n}_{\mathrm{PGAN}}$ and y_i^{PGAN}, of the waste stream, $\dot{n}_{\mathrm{Waste}}$ and y_i^{Waste}, and of the withdrawn stream (3), $\dot{n}_3$ and $x_i^{(3)}$, as well as the reflux flow rate $\dot{n}_8$ are measured. Additionally, we assume that the wall temperatures in the heat exchangers are measured, which enables direct state feedback for these units. This assumption enables a direct evaluation of the combined framework of model reduction and state estimation for the distillation column decoupled from the effects of state estimation for the heat exchangers.

All computations are run on a desktop computer with Intel® Core™ i5-8500 at 3.0 GHz and 16 GB RAM. The dynamic optimizations and simulations are performed with our open-source dynamic optimization framework DyOS [34], where we combine the integrator sLimex [39] and the NLP solver SNOPT [40]. Optimization and feasibility tolerances are set to 10^{-3}, the integration tolerance is set to 10^{-5}. The NMPC algorithm is implemented in Python, where DyOS is called through its Python interface. We employ the EKF from the `FilterPy` package [41]. The plant and controller models are implemented in the modeling language Modelica [42] and translated and accessed through the Functional Mock-up Interface [43] using Dymola [44]. We scale all model inputs and outputs to improve numerical properties in optimization.

4.2 Description of the Case Study

The study is performed in-silico, i.e., the real plant is represented by the mechanistic FOM. We consider a series of step changes in the gaseous nitrogen product demand $\dot{n}_{\mathrm{PGAN,sp}}$ as illustrated by Fig. 4. The production target changes are not known in advance. To assess the performance of the NMPC embedding the reduced model (NMPC-TWPM), we compare its closed-loop behavior to an NMPC using

the mechanistic model and full state feedback for control (NMPC-FOM). Both NMPC implementations solve the DOP (10) to convergence. Even though generally relevant for controller performance, the effect of delayed feedback is neglected in the closed-loop simulations. However, we discuss the computational cost associated with the different embedded models to evaluate the real-time capability of the strategies. We initialize the controlled system in steady-state operation with $\dot{n}_{\mathrm{Air}} = 800\,\mathrm{mol\,s^{-1}}$, $\xi_{\mathrm{side}} = 0.505$ and $\xi_{\mathrm{LIN}} = 0.001125$ at 9 ppb impurity.

Table 2: NMPC tuning parameters.

Parameter	**Value**
Δt_{s}	2.5 min
T_{u}	20 min
T_{p}	1 h
ω_1	$1\,\mathrm{sec^2\,mol^{-2}}$
ω_2	$1\,\mathrm{ppb^{-2}}$
ω_3	$1\,\mathrm{sec^2\,mol^{-2}}$

Table 2 collects the NMPC settings. Suitable controller sampling time and control grid were determined heuristically, taking into account the fast as well as slow modes of the open-loop process response. The tuning applied herein is in line with the literature on NMPC of ASUs, cf., e.g., [4]. We find the controller to be stabilizing in all load change scenarios considered in this work. As tracking of the PGAN demand is the primary objective of the controller, the weight ω_2 for the purity is tuned comparably soft to allow temporary over-purification in load change situations. The chosen value for ω_3 was found to be sufficiently large to avoid extensive utilization of the LIN stream. We further set the quality target to $x^{\mathrm{PGAN}}_{\mathrm{N_2,sp}} = 1 - (10\,\mathrm{ppb})$ for all times to operate the process at the upper quality limit. Tuning of the EKF was performed heuristically. The constraints of the DOP are summarized in Table 3. In addition to the quality requirement, we impose path constraints on the column section holdups. Moreover, we define the power ratio ζ to characterize the coupling of turbine and compressor:

$$\zeta(t) := \frac{P_{\mathrm{comp}}(t)}{P_{\mathrm{turb}}(t)}, \tag{12}$$

and constrain its values to the physically meaningful range.

Table 3: Input and state path constraints, represented by the sets $\mathcal{U}$ and $\mathcal{X}$. $\dot{n}_{\mathrm{Air}}$ feed air stream, ξ_{side} split factor side withdrawal, ξ_{LIN} split factor liquid product discharge, $1 - x^{\mathrm{PGAN}}_{\mathrm{N_2}}$ impurity, ζ power ratio of coupled compressor and turbine, $n_{\mathrm{total},1}$ liquid holdup of rectifying section, $n_{\mathrm{total},2}$ liquid holdup of stripping section.

Variable	**Lower bound**	**Upper bound**	**Type**
$\Delta\dot{n}_{\mathrm{Air}}$	$-0.2\,\mathrm{mol\,sec^{-2}}$	$0.2\,\mathrm{mol\,sec^{-2}}$	Input
$\Delta\xi_{\mathrm{side}}$	$-5\cdot10^{-4}\,\mathrm{s^{-1}}$	$5\cdot10^{-4}\,\mathrm{s^{-1}}$	Input
$\Delta\xi_{\mathrm{LIN}}$	$-10^{-4}\,\mathrm{s^{-1}}$	$10^{-4}\,\mathrm{s^{-1}}$	Input
$\dot{n}_{\mathrm{Air}}$	$600\,\mathrm{mol\,sec^{-1}}$	$900\,\mathrm{mol\,sec^{-1}}$	Path
ξ_{side}	0.48	0.52	Path
ξ_{LIN}	0	0.005	Path
$1 - x^{\mathrm{PGAN}}_{\mathrm{N_2}}$	0 ppb	10 ppb	Path
$n_{\mathrm{total},1}$	60 kmol	90 kmol	Path
$n_{\mathrm{total},2}$	6 kmol	9.5 kmol	Path
ζ	0	1	Path

4.3 Results and Discussion

In this section, we compare the results of the NMPC implementations using the reduced and full-order controller model with regard to computational time, constraint satisfaction and tracking error. Fig. 5

depicts the closed-loop trajectories of the controlled system. Fig. 5a shows the tracking performance of the controllers. Both NMPC strategies successfully accomplish tracking of the product demand with no steady-state offset. The negative steps in the production rate at $t = 2.5\,\mathrm{h}$ and $t = 7.5\,\mathrm{h}$ are tracked almost instantaneously with insignificant lag. On the other hand, the process is not able to instantaneously respond to the positive 20 % target change at $t = 5\,\mathrm{h}$. In order to satisfy the purity goal, higher production rates necessitate an increased liquid process holdup, Figs. 5c and 5d, which is provided by internal liquefication in the energy integrated process. The ramp profile of approx. 1.5 h duration can be attributed to the hard purity constraint being active, Fig. 5b, and the active input constraint for ξ_{side}, Fig. 5e, while increasing the liquid holdup. A similar behavior was found, e.g., in [45].

We observe in Fig. 5b that a bounded violation in product purity of less than 10 ppb occurs for the NMPC-TWPM case. Modification of the EKF tuning did not eliminate of this offset. Considering the wide range of concentrations in the process and the discussion in Section 3, this mismatch is generally acceptable, but may still be critical for operation of the ultra-high-purity process. However, the bounded drift appears on a relatively long time scale and is of small magnitude. Hence, we can introduce simple corrective measures to eliminate this offset. Possible strategies are an adjusted parameter fitting, e.g., by consideration of multiple steady states as discussed in Section 3.3, the definition of a conservative backoff in the NMPC cost function and constraints or the application of an offset-free NMPC method [46]. Here, we implement a systematic approach to eliminate the offset by means of adding an output bias term on the NMPC purity setpoint and consistently tighten the upper purity constraint, similar to the output disturbance model proposed by Pannocchia and Rawlings [47]. We choose this strategy as it neither increases model complexity nor requires an advanced parameter estimation strategy. This bias is defined as the difference in measured purity and model prediction and is updated at every controller sampling instant. Figs. 5a and 5b show the closed-loop tracking trajectories of the NMPC-TWPM+Bias configuration. In practice, the occasional minor overshoot in purity, which also causes a temporary fluctuation in $\dot{n}_{\mathrm{PGAN}}$, could be addressed by means of an additional small backoff. However, we do not implement such a backoff to retain comparability of the results.

Except from the purity offset, all controllers are able to satisfy the constraints in open-loop predictions and closed-loop operation at all times. Figs. 5c and 5d illustrate the trajectories of the liquid holdups. The TWPM accurately predicts the holdups and exiting streams of the column sections. In all cases, a drift in the holdups is not present, i.e., the inventories are successfully regulated by NMPC-TWPM.

The control profiles are shown in Figs. 5e to 5g. The piecewise-linear continuous parameterization provides smooth control trajectories. Both controller models, TWPM and FOM, lead to similar control profiles in all operating situations. The control action generated by the NMPC-TWPM + Bias is slightly more aggressive due to corrective action necessary for respecting the purity constraint. As a result of the additional cost term on the discharged liquid nitrogen stream $\dot{n}_{\mathrm{LIN}}$, the input constraint on the split factor ξ_{LIN} is not reached at any point and is operated close to zero most of the time.

Table 4: CPU times for online dynamic optimization. Mean reduction is calculated based on averaged CPU times.

	∅ CPU time	**Max. CPU time**	**∅ Reduction**
NMPC-FOM	57.9 sec	2728 sec	–
NMPC-TWPM	9.0 sec	139 sec	84 %
NMPC-TWPM + Bias	10.7 sec	144 sec	82 %

Table 4 shows the computational costs of the NMPC setups. Employing the reduced controller model results in an average CPU time reduction of 84 % for NMPC-TWPM, and 82 % for NMPC-TWPM + Bias. Moreover, the average and maximum CPU times of the NMPC-TWPM lie within a range of few seconds and minutes, respectively. For all controllers, the maximum CPU times were observed at time instants where the load change is realized. Here, recomputation of the optimal solution at the controller sampling points is associated with high computational cost. On the other hand, CPU times during near-stationary operation are significantly smaller as the shift initialization strategy already provides a

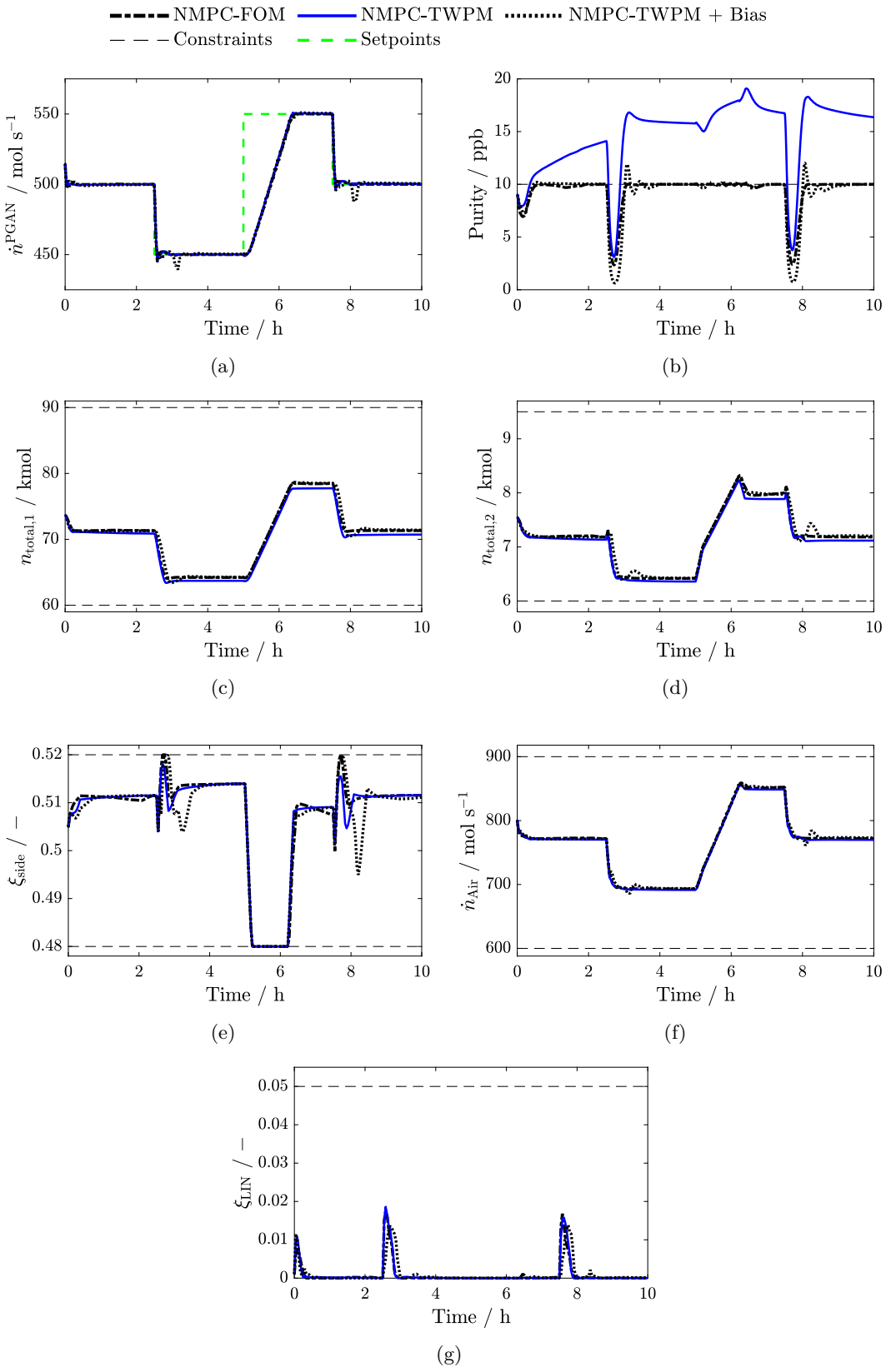

Fig. 5: Closed-loop results of control case study. (a): Molar production rate of ultra-pure gaseous nitrogen, (b): Purity of the nitrogen (PGAN) product, (c) + (d): Liquid holdups of the rectification and stripping section, respectively (path constraints). (e) + (f) + (g): Closed-loop control trajectories of the case study (MVs).

near-optimal initial guess, leading to a disparity in maximum and average CPU times in all cases. For the $\Delta t_s = 150\,\text{sec}$ controller sampling grid, all control updates are provided within one sampling interval. By contrast, NMPC-FOM exceeds a multiple of the sampling interval length in the worst case. This computational delay is prohibitive for real-time applicability. The mean computation time of NMPC-FOM lies within one sampling interval, however, even in this case introducing a delay that can generally be expected to degrade the control performance.

The worst-case CPU times of NMPC-TWPM are regarded as uncritical for the undisturbed process investigated. In general, however, control performance for processes with significant unpredicted disturbances would suffer from such computational delays. NMPC of such processes may thus require the combination of model reduction approaches and suboptimal fast-update methods [48], which only perform a limited number of iterations in the optimization. Further, when using sensitivity-based fast-update methods for control of complex flowsheets, model reduction by means of TWPM opens a way to cheap second-order sensitivity computations.

5 Conclusions and Outlook

Achieving real-time capable NMPC for large-scale chemical processes is challenging, mainly due to complex nonlinear process models. In the present study, we demonstrate that our recently introduced transient wave propagation approach is suitable for reduced modeling of multi-section multi-component ultra-high-purity distillation columns embedded in entire flowsheets. To this end, we derive a low-order controller model of a highly energy-integrated ultra-high-purity air separation process by combining TWPMs for each distillation column section.

The performance of the reduced-model NMPC is investigated in an in-silico tracking control case study. Employing the TWPM for prediction in an NMPC architecture facilitates control of production targets and process inventories in load change scenarios in the presence of strict requirements on product quality. Comparison of the controller with an NMPC embedding a full-order mechanistic model demonstrates an average CPU time reduction of 84 % and maximum CPU times within the controller sampling rate at similar closed-loop performance. A minor offset in the form of a slow and bounded drift in the predicted purity is observed as a result of plant-model mismatch. However, this offset is removed by adding an output bias on the purity setpoint and constraints, thereby enabling tight operation at the 10 ppb impurity limit. We hence conclude that the TWPM achieves strong model reduction capabilities and high accuracy that enable real-time capable NMPC in applications of industrial relevance. As the average and maximum computation times in our study lie in the range of few seconds and minutes, the extension to even more complex process topologies appears promising. Finally, coupling of model reduction and fast-update NMPC methods opens a way to further decrease in the worst-case computational delay of the control updates in cases where delayed feedback is critical.

Acknowledgements The authors gratefully acknowledge the financial support of the Kopernikus project SynErgie by the Federal Ministry of Education and Research (BMBF) and the project supervision by the project management organization Projektträger Jülich. Further, the authors would like to thank Anna-Maria Ecker (Linde GmbH) and Yannic Vaupel (AVT.SVT) for fruitful discussions and proof-reading.

References

[1] W. Marquardt, "Nonlinear model reduction for optimization based control of transient chemical processes," *AIChE Symposium Series*, 2002.

[2] S. Bian, S. Khowinij, M. A. Henson, P. Belanger, and L. Megan, "Compartmental modeling of high purity air separation columns," *Computers & Chemical Engineering*, vol. 29, no. 10, pp. 2096–2109, 2005.

[3] S. Bian, M. A. Henson, P. Belanger, and L. Megan, "Nonlinear state estimation and model predictive control of nitrogen purification columns," *Industrial & engineering chemistry research*, vol. 44, no. 1, pp. 153–167, 2005.

[4] Z. Chen, M. A. Henson, P. Belanger, and L. Megan, "Nonlinear model predictive control of high purity distillation columns for cryogenic air separation," *IEEE transactions on control systems technology*, vol. 18, no. 4, pp. 811–821, 2010.

[5] A. Caspari, C. Tsay, A. Mhamdi, M. Baldea, and A. Mitsos, "The integration of scheduling and control: Top-down vs. bottom-up," *Journal of Process Control*, vol. 91, pp. 50–62, 2020.

[6] M. Baldea and I. Harjunkoski, "Integrated production scheduling and process control: A systematic review," *Computers & Chemical Engineering*, vol. 71, pp. 377–390, 2014.

[7] K. T. Wong and R. Luus, "Model reduction of high–order multistage systems by the method of orthogonal collocation," *The Canadian Journal of Chemical Engineering*, vol. 58, no. 3, pp. 382–388, 1980.

[8] W. E. Stewart, K. L. Levien, and M. Morari, "Simulation of fractionation by orthogonal collocation," *Chemical Engineering Science*, vol. 40, no. 3, pp. 409–421, 1985.

[9] A. Benallou, D. E. Seborg, and D. A. Mellichamp, "Dyanmic compartmental models for separation processes," *AIChE Journal*, vol. 32, no. 7, pp. 1067–1078, 1986.

[10] J. Lévine and P. Rouchon, "Quality control of binary distillation columns via nonlinear aggregated models," *Automatica*, vol. 27, no. 3, pp. 463–480, 1991.

[11] W. Marquardt, "Traveling waves in chemical process," *International chemical engineering*, vol. 30, no. 4, pp. 585–606, 1990.

[12] Y.-L. Hwang, "Nonlinear wave theory for dynamics of binary distillation columns," *AIChE Journal*, vol. 37, no. 5, pp. 705–723, 1991.

[13] N. P. Hankins, "A non-linear wave model with variable molar flows for dynamic behaviour and disturbance propagation in distillation columns," *Chemical Engineering Research and Design*, vol. 85, no. 1, pp. 65–73, 2007.

[14] A. Kienle, "Low-order dynamic models for ideal multicomponent distillation processes using nonlinear wave propagation theory," *Chemical Engineering Science*, vol. 55, no. 10, pp. 1817–1828, 2000.

[15] A. Caspari, C. Offermanns, A. M. Ecker, M. Pottmann, G. Zapp, A. Mhamdi, and A. Mitsos, "A Wave Propagation Approach for Reduced Dynamic Modeling of Distillation Columns: Optimization and Control," *Journal of Process Control*, vol. 91, pp. 12–24, 2020.

[16] M. Han and S. Park, "Control of high–purity distillation column using a nonlinear wave theory," *AIChE Journal*, vol. 39, no. 5, pp. 787–796, 1993.

[17] J. Shin, H. Seo, M. Han, and S. Park, "A nonlinear profile observer using tray temperatures for high-purity binary distillation column control," *Chemical Engineering Science*, vol. 55, no. 4, pp. 807–816, 2000.

[18] A. Rehm and F. Allgower, "Nonlinear H∞-control of a high purity distillation column," *UKACC International Conference on Control*, pp. 1178–1183, 1996.

[19] L. S. Balasubramhanya and F. J. Doyle III, "Nonlinear control of a high–purity distillation column using a traveling–wave model," *AIChE Journal*, vol. 43, no. 3, pp. 703–714, 1997.

[20] G.-Y. Zhu, M. A. Henson, and L. Megan, "Low-order dynamic modeling of cryogenic distillation columns based on nonlinear wave phenomenon," *Separation and Purification Technology*, vol. 24, no. 3, pp. 467–487, 2001.

[21] X. Liu, L. Cong, and Y. Zhou, "Nonlinear model predictive control based on wave model of high-purity internal thermally coupled distillation columns," *Industrial & engineering chemistry research*, vol. 52, no. 19, pp. 6470–6479, 2013.

[22] Y. Fu and X. Liu, "An advanced control of heat integrated air separation column based on simplified wave model," *Journal of Process Control*, vol. 49, pp. 45–55, 2017.

[23] L. Cong and X. Liu, "Nonlinear-Model-Based Control of a Heat Integrated Distillation Column Using Model Updating Based on Distributed Wave Velocity," *Industrial & engineering chemistry research*, vol. 58, no. 45, pp. 20758–20768, 2019.

[24] Y. Cheng, Z. Chen, M. Sun, and Q. Sun, "Decoupling control of high-purity heat integrated distillation column process via active disturbance rejection control and nonlinear wave theory," *Transactions of the Institute of Measurement and Control*, p. 0142331220908989, 2020.

[25] M. Han and S. Park, "Startup of distillation columns using profile position control based on a nonlinear wave model," *Industrial & engineering chemistry research*, vol. 38, no. 4, pp. 1565–1574, 1999.

[26] Y. Cao, C. Swartz, and J. Flores-Cerrillo, "Optimal dynamic operation of a high-purity air separation plant under varying market conditions," *Industrial & engineering chemistry research*, vol. 55, no. 37, pp. 9956–9970, 2016.

[27] A. Kumar and P. Daoutidis, "Nonlinear model reduction and control for high-purity distillation columns," *Industrial & engineering chemistry research*, vol. 42, no. 20, pp. 4495–4505, 2003.

[28] S. Grüner, S. Schwarzkopf, I. Uslu, A. Kienle, and E. D. Gilles, "Nonlinear model predictive control of multicomponent distillation columns using wave models," *ADCHEM2004: 7th International symposium on advanced control of chemical processes Hong Kong*, pp. 231–236, 2004.

[29] S. Schwarzkopf, *Echtzeitfaehige optimierungsbasierte Regelung von Stofftrennprozessen*. Dissertation, Otto-von-Guericke-Universitaet, Magdeburg, 2012.

[30] P. Schäfer, A. Caspari, A. Mhamdi, and A. Mitsos, "Economic nonlinear model predictive control using hybrid mechanistic data-driven models for optimal operation in real-time electricity markets: In-silico application to air separation processes," *Journal of Process Control*, vol. 84, pp. 171–181, 2019.

[31] H.-W. Häring and A. Belloni, *Industrial gases processing*. John Wiley & Sons, 2008.

[32] J. P. Naumovitz, "Air separation method and apparatus for producing nitrogen," 1996.

[33] W. Marquardt, "Nonlinear model reduction for binary distillation," *Dynamics and Control of Chemical Reactors and Distillation Columns*, pp. 123–128, 1986.

[34] A. Caspari, A. Bremen, J. M. Faust, F. Jung, C. D. Kappatou, S. Sass, Y. Vaupel, R. Hannemann-Tamás, A. Mhamdi, and A. Mitsos, "DyOS-a framework for optimization of large-scale differential algebraic equation systems," in *Computer Aided Chemical Engineering*, vol. 46, pp. 619–624, Elsevier, 2019.

[35] A. Kienle, E. Stein, A. Rehm, and E. Kloppenburg, "Low-order dynamic models for two coupled distillation columns," *1999 European Control Conference (ECC)*, pp. 3059–3064, 1999.

[36] J. B. Rawlings, D. Q. Mayne, and M. Diehl, *Model predictive control: theory, computation, and design*. Nob Hill Publishing Madison, WI, 2017.

[37] S. Skogestad, "The dos and don'ts of distillation column control," *Chemical Engineering Research and Design*, vol. 85, no. 1, pp. 13–23, 2007.

[38] V. M. Becerra, P. D. Roberts, and G. W. Griffiths, "Applying the extended Kalman filter to systems described by nonlinear differential-algebraic equations," *Control Engineering Practice*, vol. 9, no. 3, pp. 267–281, 2001.

[39] M. Schlegel, W. Marquardt, R. Ehrig, and U. Nowak, "Sensitivity analysis of linearly-implicit differential–algebraic systems by one-step extrapolation," *Applied Numerical Mathematics*, vol. 48, no. 1, pp. 83–102, 2004.

[40] P. E. Gill, W. Murray, and M. A. Saunders, "SNOPT: An SQP algorithm for large-scale constrained optimization," *SIAM review*, vol. 47, no. 1, pp. 99–131, 2005.

[41] R. R. Labbe, JR, "FilterPy." https://filterpy.readthedocs.io/, accessed 2020.

[42] Modelica Association, "Modelica." https://www.modelica.org/, accessed 2020.

[43] Modelica Association, "Functional Mock-Up Interface (FMI)." https://fmi-standard.org/, accessed 2020.

[44] Dassault Systemes, "Dymola 2018 64-bit." https://www.3ds.com/products-services/catia/products/dymola/, accessed 2020.

[45] Y. Cao, C. L. Swartz, M. Baldea, and S. Blouin, "Optimization-based assessment of design limitations to air separation plant agility in demand response scenarios," *Journal of Process Control*, vol. 33, pp. 37–48, 2015.

[46] M. Morari and U. Maeder, "Nonlinear offset-free model predictive control," *Automatica*, vol. 48, no. 9, pp. 2059–2067, 2012.

[47] G. Pannocchia and J. B. Rawlings, "Disturbance models for offset-free model-predictive control," *AIChE journal*, vol. 49, no. 2, pp. 426–437, 2003.

[48] I. J. Wolf and W. Marquardt, "Fast NMPC schemes for regulatory and economic NMPC–A review," *Journal of Process Control*, vol. 44, pp. 162–183, 2016.